Dynamic Modeling of Ring Nutation Dampers

Reid Reynolds*
Spectrum Astro, Inc., Herndon, Virginia 20170

Introduction

RECENTLY published analyses of nutation dampers are not widely available, but modeling damper performance is an interesting problem combining many disciplines. This Note presents a new perspective on nutation dampers such as the one examined in Ref. 1. There, the damper consisted of a hoop of metal partially filled with a viscous fluid and mounted in the spacecraft spin plane, with both horizontal and vertical offsets from the spacecraft center of gravity.

For small nutation angles the fluid slug is held intact and toward the outer edge of the hoop by the centrifugal force. Small oscillations are induced at the nutation frequency, and viscous forces dissipate energy. Large nutation angles produce rectified torques that propel the slug around the hoop. Although there is a component of steady flow in this case, the dissipative torques at harmonics of the spin and nutation rates can play a significant role in the overall damping of the nutation.

The most important parameter for modeling the action of a fluid-based nutation damper is the kinetic Reynolds number.[2] For unsteady flow this quantity plays a similar role to the standard Reynolds number of steady flow theory in defining regions of laminar and turbulent flow.

Unsteady flow regimes typically dominate for low viscosity fluids. However, one low viscosity fluid that has been used extensively in nutation dampers, mercury, has the disadvantage of exhibiting high surface tension. Surface tension has been demonstrated to cause small angle "lock-up," in which the damper ceases to dissipate energy below a particular nutation angle.[3] This Note does not model effects of surface tension, but evaluation of the potential for small angle lock-up is recommended in general applications.

The shear stress in an unsteady flow regime is generally much larger than that in a steady flow situation, and this fact can be used to advantage in designing faster nutation dampers. One salient feature of the unsteady flow regime is that the damping turns out to be proportional to the square root of the fluid viscosity, rather than directly proportional as might be expected. A simple experimental apparatus is sufficient to demonstrate the validity of the analysis.

Fluid Dynamics

The damper model is as depicted in Fig. 1. Assuming $b \gg a$, the Navier–Stokes equation for the fluid velocity V is approximately

$$\frac{\partial V}{\partial t} - \nu\left(\frac{\partial^2 V}{\partial r^2} + \frac{1}{r}\frac{\partial V}{\partial r}\right) = Ae^{st} \tag{1}$$

for kinematic viscosity ν, annular radius r, and a general complex exponential pressure gradient with amplitude A and Laplace variable s. The solution of Eq. (1) is given in Ref. 2:

$$V = \left[1 - \frac{J_0\left(r\sqrt{-s/\nu}\right)}{J_0\left(a\sqrt{-s/\nu}\right)}\right]\frac{A}{s}e^{st} \tag{2}$$

where $J_n(\,)$ is the nth-order Bessel function of the first kind with complex argument.[2,4–7] The argument of this function is related to the kinetic Reynolds number[2] (KRN)

$$R_\omega = \omega a^2/\nu \tag{3}$$

where ω is the oscillation frequency of the fluid slug. For convenience, we shall define the analogous Laplace version

$$R_s = (a^2/\nu)s \tag{4}$$

For purely simusoidal forcing functions the fluid flow is laminar for R_ω of less than about 2000.[2] As R_s approaches zero (low frequency, high viscosity, and/or small annulus), Eq. (2) approaches the steady-state limit

$$V \underset{R_s \to 0}{\to} \frac{A}{4\nu}(a^2 - r^2) \tag{5}$$

which is the familiar parabolic shape of the velocity distribution in steady pipe flow. Because fluid viscosities can be quite small, it is not difficult to have a large KRN. The velocity distributions in this case are markedly different from Eq. (5), as shown in Fig. 2.

The average velocity of the slug over the cross-sectional area is

$$V_{\text{avg}} = \left[1 - \frac{2J_1\left(j\sqrt{R_s}\right)}{j\sqrt{R_s}J_0\left(j\sqrt{R_s}\right)}\right]\frac{A}{s}e^{st} \tag{6}$$

where j is the square root of -1.

The higher-Reynolds-number cases have dramatically greater increases in the velocity near the tube wall, leading to significantly higher shear stresses. The shear stress can be calculated as

$$\sigma = \rho\nu\left.\frac{\partial V}{\partial r}\right|_{r=a}$$

where ρ is the fluid density. The result is

$$\sigma = \frac{\rho\nu}{a}j\sqrt{R_s}\frac{J_1\left(j\sqrt{R_s}\right)}{J_0\left(j\sqrt{R_s}\right)}\frac{A}{s}e^{st} \tag{7}$$

The torque about the center of the hoop is found by multiplying Eq. (7) by the surface area S of the fluid slug touching the tube walls, and the moment arm b, $\tau = bS\sigma$.

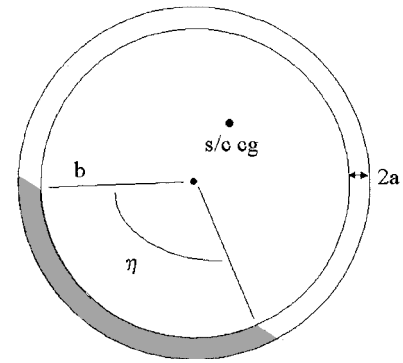

Fig. 1 Offset partially filled ring nutation damper.

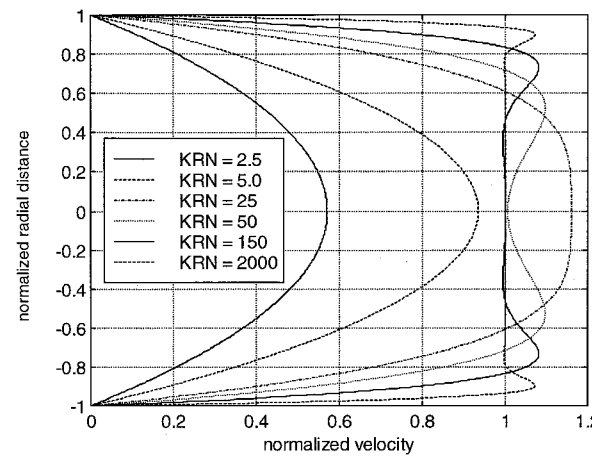

Fig. 2 Selection of velocity profiles for varying KRN.

Received 20 September 2001; revision received 6 May 2002; accepted for publication 30 August 2002.

*Senior ACS Engineer, 2214 Rock Hill Road, Suite 101. Member AIAA.

Defining $b\dot{\phi} = V_{\text{avg}}$, the transfer function between $\dot{\phi}$ and τ becomes

$$\frac{\tau(s)}{\dot{\phi}(s)} = \frac{-C\nu R_s J_1\left(j\sqrt{R_s}\right)}{j\sqrt{R_s}J_0\left(j\sqrt{R_s}\right) - 2J_1\left(j\sqrt{R_s}\right)} \tag{8}$$

where $C = 2\pi\rho\eta b^3$. Despite the appearance of j in Eq. (8), the function is real for real s. Henceforward, we shall identify this transfer function as $-F(s)$.

In the first limiting case of interest, when R_s is "small," the transfer function becomes a constant

$$F(s) \approx 4C\nu \tag{9a}$$

and, when R_s is "large"

$$F(s) \approx C\nu\sqrt{R_s} = Ca\sqrt{\nu s} \tag{9b}$$

in which the dependence of the damping on the square root of the viscosity appears. In this regime a rational approximation of the square-root function of s yields a transfer function easily implemented in simulations. Because it can be presumed that the excitation of the slug will occur at the nutation frequency ω_n of the spacecraft, a first-order lead filter that has the same magnitude and phase at $s = j\omega_n$ is

$$\sqrt{s} \approx \frac{\sqrt{\omega_n}}{\alpha}\frac{s/(\omega_n/\alpha)+1}{s/(\omega_n\alpha)+1}, \qquad \alpha = 1+\sqrt{2} \tag{10}$$

In Figs. 3 and 4 the magnitude and phase of $-F(j\omega)/C\nu$ vs R_ω are plotted with dashed line asymptotes given by Eq. (9b).

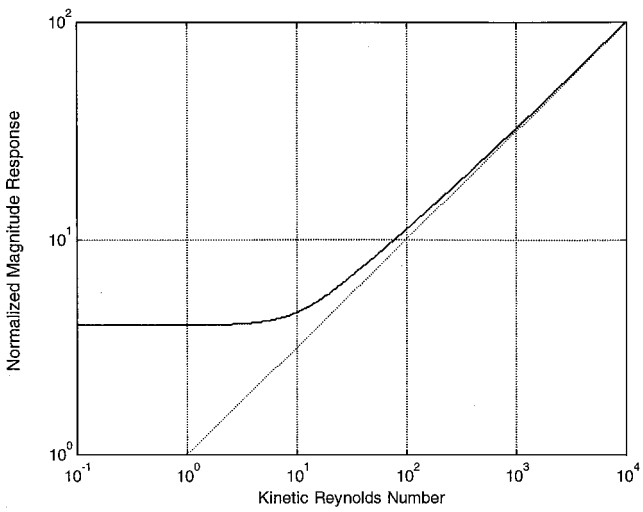

Fig. 3 Magnitude response of fluid dynamics transfer function.

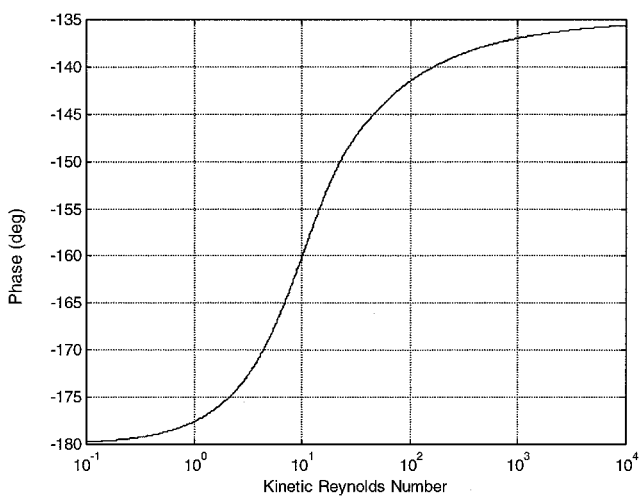

Fig. 4 Phase response of fluid dynamics transfer function.

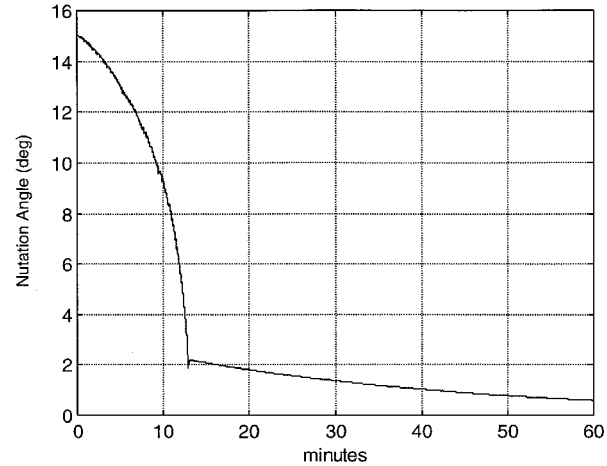

Fig. 5 Nutation angle decay caused by damper.

As can be seen, Eq. (9b) is not very far off for KRN greater than about 10. One of the insights revealed by the phase plot is that the fluid dynamics has a leading response. Another important insight is the amplification that occurs for high KRN. As the KRN is proportional to frequency, it is possible that the higher frequency components dominate the damping during large-angle nutation.

Simulations

For simulation a rigid body with offset damper, characterized as a single-degree-of-freedom solid pendulum with the damping torque response given by the rational approximation in Eq. (10), was modeled.

In the plot shown in Fig. 5, an initial nutation angle of 15 deg decays because of the action of the damper. In the large-angle regime (>2 deg for this case), the damping rate is faster owing, perhaps, to the input frequency spread, which includes harmonics and modulations of the nutation and spin rates, as well as dc components from rectification phenomena. The simulation model might not be entirely accurate for this multimode regime because the damping torque is based on Eq. (10), but the behavior is similar to that described elsewhere[8] (although, in that case, attributed to turbulent flow phenomena).

After about 2 deg nutation angle is reached, the slug rate is essentially composed of one harmonic at the nutation frequency, and so Eq. (10) is a reasonable model for the fluid response. The damping torque becomes proportional to a phase-advanced version of the rate, and the decay becomes exponential.

Experiment

Based on the suspicion that the predicted phenomena should be strongly observable, a very simple and easily replicated test apparatus was constructed to observe the damping predictions. The apparatus was crude, and any measure of the absolute accuracy of the results would be speculative. However, the differences in performance for the various configurations were so dramatic as to leave little doubt that the predictions had been confirmed.

The diagram in Fig. 6 depicts a half-hoop of copper tubing, such as is easily purchased at a local hardware store. Four hoops were suspended with coat hanger wires, each looped through an eyelet constructed of the same wire, creating a low friction interface. The hoops were filled with various fluids and induced to rock back and forth. The times for the oscillations to decay to a nearly unobservable angle were then recorded and compared with the predictions.

The fluid slug was modeled as a solid pendulum, and the linearized equations of motion came out to be approximately

$$G\begin{bmatrix}\ddot{\theta}\\ \ddot{\phi}\end{bmatrix} + H\begin{bmatrix}\theta\\ \phi\end{bmatrix} = \begin{bmatrix}0\\ \tau_f\end{bmatrix} \tag{11}$$

for appropriate constant 2×2 matrices G and H with τ_f equal to the damping torque. The determinant of the Laplace transform of

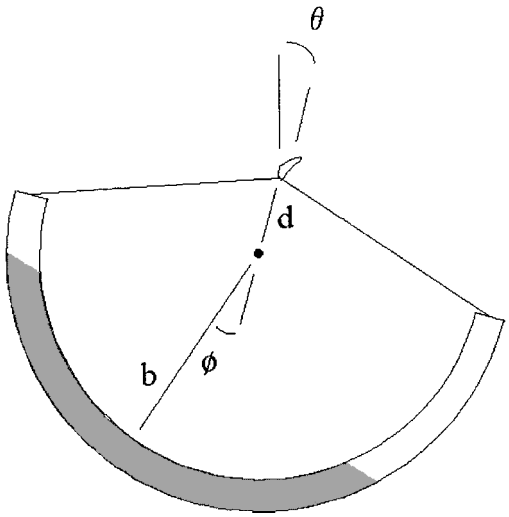

Fig. 6 Experimental setup.

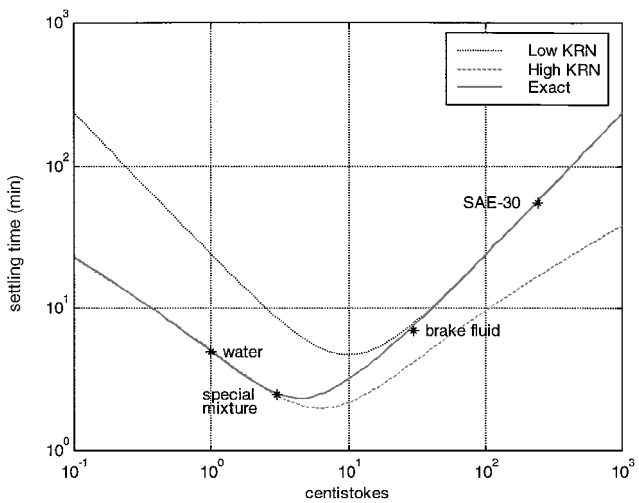

Fig. 7 Experimental settling times closely match model.

Eq. (11) is the characteristic equation

$$\Delta(s) = \left| Gs^2 + H + \begin{bmatrix} 0 & 0 \\ 0 & sF(s) \end{bmatrix} \right| \tag{12}$$

The frequency ω_n of oscillation can be predicted. For low viscosity fluids (high KRN), it was found that the pendulum frequency of the copper tubing alone was predominant. For high viscosity fluids (low KRN), the pendulum frequency of the combined tubing and fluid was predominant. Given the frequency ω_n of oscillation, the time constant of the damping can be predicted by using the analyticity of Eq. (12):

$$\tau_{\text{damp}} = 1/\{\text{Real}[\Delta(j\omega_n)/\Delta'(j\omega_n)]\} \tag{13}$$

In Fig. 7 this equation was applied using Eqs. (9) for the low- and high-KRN cases, respectively, and the appropriate pendulum frequency. The actual settling time (solid line) was found by setting Eq. (12) to zero and solving, using a Newton iteration and the full fluid transfer function in Eq. (8). With just a minor tweaking of parameters, the observed settling times closely matched the analytically derived settling times.

The dashed line for the low-KRN case is essentially what would be obtained using the steady flow equations. Note how much more rapid the damping can be for the high-KRN solution. For the case in which water was used as the damping medium, the settling time was almost a full order of magnitude less than that predicted by the steady-state pipe flow (low KRN) curve, providing dramatic confirmation of the unsteady flow model.

Upon noting that the graph suggested that the minimum settling time could be achieved for a fluid slightly more viscous than water, the coffee service was raided, and a saturated solution of sugar and water was combined into the "special mixture." The result was a significantly reduced settling time, as predicted.

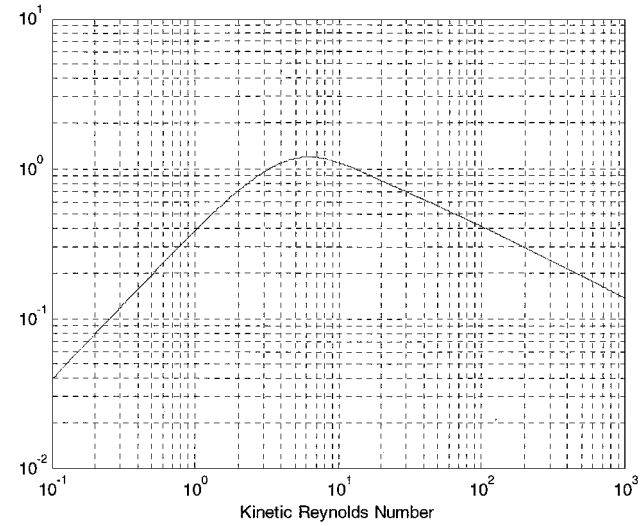

Fig. 8 Normalized energy dissipation function.

Comparison with Earlier Results

As stated in the Introduction, there do not appear to be many recent analyses of nutation dampers published in the literature. One past analysis of particular note is the 1966 Bhuta and Koval paper,[9] which derives the time constant for a nutating spacecraft with a fully filled ring damper with the axis of symmetry mounted along a transverse body axis. Although Bhuta and Koval derived their result in an entirely different manner using energy sink methods, their result agrees precisely with that predicted by the transfer function approach adopted here. A significant advantage of the transfer function approach is that, with suitable rational approximation of Eq. (8), the performance of nutation dampers for complex multibody systems not amenable to analytic solution can be predicted through simulation.

A small-angle linearization of the nutation dynamics analyzed by Bhuta and Koval leads to the characteristic equation given by

$$\Delta(s) = J_t[J_f s + F(s)]\left(s^2 + \omega_n^2\right) + J_f^2 s\left(\omega_n \omega_s - s^2\right) \tag{14}$$

where J_t is the transverse spacecraft inertia, J_f is the inertia of the fluid about the symmetric axis ($\approx mb^2$ for a thin tube, where m is the mass of the fluid and b is the hoop radius), ω_s is the spin frequency, ω_n is the nutation frequency, $\omega_n = (J_s/J_t - 1)\omega_s$, and J_s is the spacecraft spin axis (major axis) inertia.

Plugging this characteristic equation into Eq. (13) results in

$$\tau \approx \frac{2\pi J_t^2}{f[F(j\omega_n)/J_f\omega_n]J_f J_s \omega_s} \tag{15}$$

where $f(z) = \pi x/[x^2 + (1+y)^2]$ for complex argument $z = x + jy$. The argument of this function in Eq. (15) depends only on the KRN and, $f[F(j\omega_n)/J_f\omega_n]$ is identical to the "normalized energy dissipation function" derived by Bhuta and Koval and plotted in Fig. 8. The minimum time constant (maximum energy dissipation) occurs for a KRN of about 6.5 at the transition from steady to unsteady flow.

Conclusions

The dynamics of fluid-filled ring nutation dampers can be described using standard linear control system conventions. The fundamental characteristic of the frequency response of these dampers is the leading phase.

The damping is generally much greater for high kinetic Reynolds numbers. This can lead to dramatically reduced settling times vs those predicted by steady flow models, if physical parameters are chosen appropriately and if surface tension lock-up is not an issue.

Acknowledgments

This study was supported by funding from Spectrum Astro IR&D, with special encouragement from Stanley Dubyn. The author thanks F. L. Markley of NASA Goddard Space Flight Center, Robert Bauer of Bauer Engineering, and Carl Hubert of Hubert Astronautics for helpful comments and suggestions.

References

[1]King, B. G., and Woolley, R. P., "Modeling, Tuning, and Effectiveness of Partially-Filled Ring Nutation Dampers," *Advances in the Astronautical Sciences*, Vol. 57, edited by R. D. Culp, E. J. Bauman, and C. A. Cullian, American Astronautical Society, Springfield, VA, 1985, pp. 431–452.

[2]Constantinescu, V. N., *Laminar Viscous Flow*, Springer-Verlag, New York, 1995, pp. 193–195.

[3]Hubert, C., and Swanson, D., "Surface Tension Lockup in the IMAGE Nutation Damper—Anomaly and Recovery," *2001 Flight Mechanics Symposium*, edited by J. P. Lynch, NASA Goddard Space Flight Center, Greenbelt, MD, 2001, p. 527.

[4]Arfken, G., *Mathematical Methods for Physicists*, Academic Press, Boston, 1985, pp. 573–584.

[5]Beyer, W. H., *CRC Standard Mathematical Tables,* CRC Press, Boca Raton, FL, 1984, pp. 349–351.

[6]Gradshteyn, I. S., and Ryzhik, I. M., *Table of Integrals, Series, and Products*, Academic Press, Boston, 1980, pp. 951–954.

[7]Kreyszig, E., *Advanced Engineering Mathematics*, Wiley, New York, 1993, pp. 225–231.

[8]Kaplan, M. H., *Modern Spacecraft Dynamics and Control*, Wiley, New York, 1976, pp. 131–139.

[9]Bhuta, P. G., and Koval, L. R., "A Viscous Ring Damper for a Freely Precessing Satellite," *International Journal of the Mechanical Sciences*, Vol. 8, 1966, pp. 383–394.

Gravity-Turn Descent from Low Circular Orbit Conditions

Colin R. McInnes*
University of Glasgow,
Glasgow, Scotland G12 8QQ, United Kingdom

Introduction

GRAVITY-TURN descent to the surface of a planetary or small solar system body has been investigated for many years and, indeed, has been used for both lunar and Mars descent vehicles.[1–5] Such a descent profile requires that the vehicle thrust vector is oriented opposite to the instantaneous velocity vector along the entire descent trajectory. This requirement can be achieved with knowledge of the vehicle velocity vector from an inertial measurement unit and an attitude control system that can maintain the thrust vector antiparallel to the instantaneous velocity vector.[1] For pure gravity-turn descent, the steering law is, therefore, relatively easy to implement in practice, although the descent may be modified at the terminal phase for surface hazard avoidance. An important benefit of gravity-turn descent is that the landing is assured to be vertical, and the steering law is close to fuel optimum.[3]

The equations of motion for gravity-turn descent can be solved in closed form for a fixed thrust-to-weight ratio, assuming that a constant, vertical gravitational acceleration is the only other force acting on the descent vehicle.[1] The latter approximation limits the validity of the solutions to regimes where the descent vehicle velocity is small relative to the local circular orbit velocity because centripetal forces are ignored. The closed-form solutions can, therefore, only be used to describe terminal descent, when the vehicle has braked from circular orbit velocity and is close to the planetary surface. In this Note, it will be demonstrated that the equations of motion for gravity-turn descent can, in fact, be solved in closed form if centripetal forces are retained, but gravity is assumed to be constant in magnitude. Because the descent will normally begin from a low circular parking orbit, these assumptions appear reasonable. New solutions are found that allow a full representation of the descent vehicle motion from circular orbit conditions down to the final landing event.

Received 4 December 2001; revision received 1 April 2002; accepted for publication 29 June 2002.

*Professor, Department of Aerospace Engineering; colinmc@aero.gla.ac.uk.

Classical Gravity-Turn Solutions

The general equations of motion for the descent vehicle can be written in normal-tangential coordinates, with the vehicle thrust-induced acceleration written as Ng_0, where N is the thrust-to-weight ratio and g_0 is the gravitational acceleration at the planetary surface, as shown in Fig. 1. For a planetary or small solar system body of radius R, the equations of motion may be written as

$$\frac{dv}{dt} = g_0 \frac{R^2}{(R+h)^2}\cos\psi - Ng_0 \tag{1a}$$

$$v\frac{d\psi}{dt} = \left\{\frac{v^2}{R+h} - g_0\frac{R^2}{(R+h)^2}\right\}\sin\psi \tag{1b}$$

$$\frac{dh}{dt} = -v\cos\psi \tag{1c}$$

where v is the vehicle velocity, ψ is the pitch angle of the vehicle velocity vector relative to the local vertical, and h is the vehicle altitude above the planetary surface. The classical gravity-turn solutions can be obtained by assuming the descent takes place over a plane so that $R \to \infty$. In this limit, the equations of motion reduce to

$$\frac{dv}{dt} = g_0\cos\psi - Ng_0 \tag{2a}$$

$$v\frac{d\psi}{dt} = -g_0\sin\psi \tag{2b}$$

These reduced equations may now be used to form a single, separable differential equation with ψ as the independent variable, such that

$$\frac{1}{v}\frac{dv}{d\psi} + \cot\psi - N\operatorname{cosec}\psi = 0 \tag{3}$$

This equation can now be directly integrated to obtain the descent vehicle velocity v as a function of the velocity vector pitch angle ψ as[1]

$$v(\psi) = v_0\left\{\frac{\sin\psi_0}{\sin\psi}\right\}\left\{\frac{\tan(\psi/2)}{\tan(\psi_0/2)}\right\}^N \tag{4}$$

A typical descent trajectory in the v–ψ plane is shown in Fig. 2 for a thrust-to-weight ratio $N = 2$, with a numerically integrated solution of Eq. (1) provided for comparison. The descent begins from circular orbit conditions. It can be seen that this closed-form solution

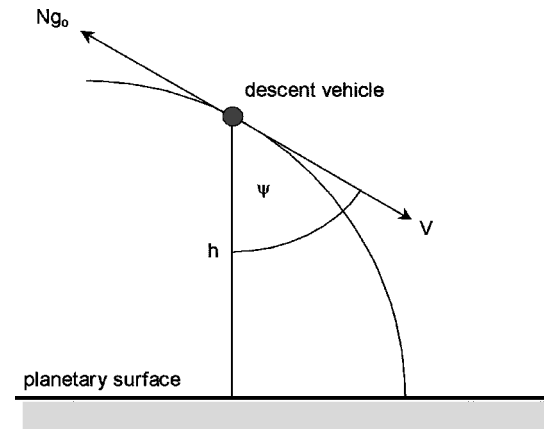

Fig. 1 Schematic of gravity-turn descent.